Trans Indian Inst Met (2019) 72(9):2477–2486
https://doi.org/10.1007/s12666-019-01701-4

TECHNICAL PAPER

Microstructural Characterization and Deformation Behavior of Zn–8Al-Cenosphere Hybrid Foam

Manoj Mohbe[1] · D. M. Afzal Khan[1] · D. P. Mondal[2]

Received: 6 October 2018 / Accepted: 28 April 2019 / Published online: 16 May 2019

Abstract Zn–8Al alloy with density 6.3 g/cm^3 was foamed by using cenosphere particles as a thickening agent and CaH_2 as foaming agent via stir-casting technique. The cenosphere particles also worked as a space holder to create microporosity into the foam structure. The relative density of the hybrid foam has been obtained in the range of 0.18–0.27. The synthesized hybrid foam was studied under microscopic evaluation and compressive deformation behavior. From scanning electron microscopic observation, it was found that cenosphere particles are dispersed into the cell walls of the hybrid foam as the strengthening material. Compressive deformation of the samples sliced from the foam ingot was examined with different conditions to find out the effect of strain rate and temperature. The properties were evaluated in terms of plateau stress, energy absorption capacity, densification strain, maximum stress and energy absorption efficiency. The present work is focused on the parameters which affect energy absorption efficiency of hybrid foam. It was noted that plateau stress and energy absorption capacity increases with relative density and strain rate. The temperature of the furnace during the compression test was varied from 100 to 250 °C and the result obtained shows that plateau stress and energy absorption capacity values reduces with an increase in temperature during the compression test. The energy absorption efficiency of the hybrid foam varies in the range of 56–90% as it depends on the compressive deformation. More constant plateau region results in higher energy absorption efficiency. Densification strain is found to be almost constant for each set of conditions.

Keywords Zn–8Al foam · Stir-casting · Cenosphere · Compressive deformation · Energy absorption efficiency

Abbreviations

RD	Relative density
PS	Plateau stress
EAC	Energy absorption capacity
EAE	Energy absorption efficiency
SR	Strain rate
DS	Densification strain
SRS	Strain rate sensitivity
CPs	Cenosphere particles

List of Symbols

ρ_{RD}	Relative density
σ_{pl}	Plateau stress
E_{ab}	Energy absorption capacity
η	Energy absorption efficiency
ε_d	Densification strain

1 Introduction

Closed cell metal foams exhibit good mechanical characteristics like stiffness and strength. It has plateau stress (PS) when subjected to compressive load and high energy absorption capacity (EAC) [1]. Metal foam materials having open pores and closed pores find applications in energy and sound absorption, automobiles, thermal insulation and aerospace. But, nowadays researchers are

✉ Manoj Mohbe
manojmohbe@gmail.com

[1] Department of Metallurgical and Materials Engineering, N.I.T, Srinagar, Jammu and Kashmir 190006, India

[2] CSIR-Advanced Materials and Processes Research Institute, Bhopal 462026, India

focusing on high-temperature applications such as heat shielder and cooling system in gas and steam turbine.

The hollow microballoons Al_2O_3 and cenosphere particles (CPs) were added to the melt by researchers to get lightweight material as syntactic foam having better properties in terms of stiffness, yield strength and PS. The Al syntactic foam was synthesized by melt infiltration technique with pressure infiltration using silica–mullite hollow microsphere and reported a significant improvement in stiffness [2]. The compressive behavior of Al syntactic foam was observed [3] and has been reported that compressive strength increased with the density (ρ), and annealed syntactic foam had higher yield strength. Hollow Al_2O_3 particles were also employed to fabricate Al syntactic foam [4]. The compression tests were already carried out at high temperature for Al syntactic foam at 100, 150 and 200 °C [5] and it was found to decrease in PS with temperature. Al particles were added to Al syntactic foam in order to improve ductility and EAC [6].

Reinforcing agent (Al_2O_3, ZnO) was added to Zn–Al alloys to get composite material. The ZnAl27 alloy matrix reinforced with Al_2O_3 particles (0, 4, 8, and 12 wt.%) was evaluated [7], and results obtained by the analysis helped us to understand de-bonding behavior between matrix interfaces. The wear volume loss of ZnAl27–nanoAl_2O_3 composite decreased with increase in reinforcing agent [8]. ZnO nanoparticles (0, 1, 2, 3, 4 and 5 wt.%) were added to ZnAl27 alloy to form low-density composite material with high performance [9] and found 4 wt.%. The sample had high tensile strength and hardness values.

Zn–Al alloys have considerable mechanical strength, softness, and lower melting point makes it suitable for energy absorption applications. The ZnAl22 composite foam was synthesized by melt foaming route using SiC (10 vol%) and $CaCO_3$ (0.3–0.6 wt%) as a foaming agent and reported improvement in damping capacity of foam [10]. The ZnAl27–SiC foam was fabricated using CaH_2 foaming agent. The foam was developed with a density of 0.25–0.45 g/cm^3, and micro-architectural properties were estimated in terms of cell size and cell wall thickness [11]. The high-temperature deformation under compressive loading was checked for ZnAl27–SiC foam with varying strain rate (SR), and results showed that compressive strength increased with a relative density (RD) and decreased with temperature [12]. The compression and tensile tests were performed for ZnAl22 foam and 0.55 strain rate sensitivity (SRS) was reported [13].

Stir-casting technique is a simple method and suitable for mass production. It requires a ceramic particle (thickening agent) such as Ca granules, SiC, CaC, CPs and Al_2O_3 to stabilize melt during foam making. Thickening agents are reinforced into melt for increasing viscosity of melt. Increase in viscosity of the melt leads to fewer chances of escape of gas bubbles formed into the melt by means of gas injection or introducing foaming agents. In addition, the thickening agent provides higher stiffness and yield strength than the corresponding matrix material [14]. The property of metal foam depends on the properties and concentration of the thickening agent. A356 (Al–7Si–0.35Mg) Al alloy foam was synthesized by melt route using Al_2O_3, $BaSO_4$ and $CaSiO_3$ as a thickening agent and it was reported that for the same concentration, $BaSO_4$ foam resulted in good structural and mechanical properties, while $CaSiO_3$ foam produced higher porosity, and the properties of Al_2O_3 foam gave intermediate values of the cell size and porosity [15]. Foaming of ZnAl12 alloy was attempted by stir-casting technique using $CaCO_3$ foaming agent with different volume percents of CPs and it was reported that high SRS and EAC increased by 90% with increasing SR [16]. The ZnAl27-cenosphere (20 vol%) hybrid foam synthesized using CaH_2 was put under compression test with varying SR and temperature [17]. The ZnAl12 hybrid foam was investigated under compression test in order to find the effect of SR and temperature and it was reported that PS and EAC increased with RD and SR but decreased with the increase in temperature [18].

CPs were added to the hybrid foam for dual applications such as thickening agent and space holder. The effect of CPs content was observed for Al hybrid foam and it was reported that the compressive strength of the hybrid foam increased up to certain addition of CPs, more addition could lead to decrease in the strength [19]. The particle size also influenced the properties of hybrid foam, i.e., lower CPs size resulted in higher compressive properties [20]. Foaming of ZnAl12 alloy was attempted by stir-casting technique using $CaCO_3$ foaming agent with different volume percents of CPs and reported that high SRS and EAC increased by 90% with increasing SR [16]. The ZnAl27-cenosphere (20 vol%) hybrid foam synthesized using CaH_2 was put under compression test with varying SR and temperature [17]. The ZnAl12 hybrid foam was investigated under compression test in order to find the effect of SR and temperature and reported that PS and EAC increased with RD and SR but decreased with increase in temperature [18].

However, Al and Mg alloys are easy to foam by using various thickening and foaming agents due to its lower density. The foaming of Zn–8Al alloy (6.3 g/cm^3 density) is quite difficult by using CPs with (0.6 g/cm^3) density because, due to density difference and hollowness of CPs, it floats on the melt on mixing and requires continuous stirring during mixing. It has been reported that lower CPs size gives higher strength and the addition of CPs for Al alloys is limited up to 30 vol%. Further increase in particle quantity leads to loss in the strength of the synthesized foam.

From the information available, we have come to learn that very few studies were carried out on the synthesis and characterization of Zn–Al hybrid foam. The ceramic particles used as thickening agent, i.e., SiC, CaC_2, Al_2O_3, etc, are relatively costly as compared to CPs. The present study is focused on the synthesis of Zn–8Al hybrid foam having density of 6.3 g/cc using CPs as a thickening agent as well as a space holder to create microporosity into the cell walls of the hybrid foam to increase EAC. The content of the CPs ($\leq$ 100 μm) has been taken as 20 Vol%.

2 Method and Experimentation

2.1 Synthesis of Foam

2.1.1 Composite Preparation

The synthesis of Zn–8Al hybrid foam was carried out at Advanced Materials Processes Research Institute (AMPRI)–CSIR, Bhopal (India). Pure Zn (92 wt.%) and Al (8 wt%) were added into induction furnace for melting at 650 °C. On melting, the components were mixed with a mechanical stirrer for 2 min for homogeneous mixing of the alloy. The preheated (600 °C for 4 h) CPs (20 vol%) of average size of 63.62 μm were added manually into the melt by mechanical stirring. The distribution of CPs is shown in Fig. 1a, and the microstructure of CPs used for making composite is shown in Fig. 1b. For uniform mixing, stirring was allowed for a significant time. After reinforcing CPs, the mix was collected in a graphite mold and allowed to solidify.

2.1.2 Foaming Operation

The prepared composite was re-melted in the induction furnace for foaming operation at 600 °C. Once the composite got melted, the stirring was applied to ensure homogeneous mixing of CPs into the melt. After that foaming agent (CaH_2 in 0.5 wt%) of 10–20 μm size was added into the melt manually through mechanical stirrer and temperature was maintained at 580–600 °C in order to get different RDs for hybrid foam. Due to the addition of CaH_2, the foaming got started and continued for 30–40 s. The crucible was then taken out from the furnace, and quick solidification of melt foam was applied using air spray to get solid hybrid foam.

2.2 Compressive Deformation Behavior

The compression test was carried out for each sample with different RDs by varying SR (0.01, 0.1 and 1 s^{-1}). The samples were placed in the heating chamber of the universal testing machine (UTM) for 15 min for uniform heating of the sample. Group G1, G2 and G3 illustrated in Table 1 represents sets of 0.27, 0.24 and 0.18 RD at constant temperature 100 °C varying strain rate from 0.01 to 1 s^{-1} to find the effect of strain rate on the compressive deformation behavior of hybrid foam. The effect of temperature was observed on the compressive deformation behavior of 0.27, 0.24 and 0.18 RD and was examined for four different temperatures (100, 150, 200 and 250 °C) as it represented G1, G2, G3, G4, G5 and G6 at constant strain rate 0.01 s^{-1}.

The stress–strain curves obtained from the compression test had three different regions, i.e., linear elastic region (stress increases with strain rate), plateau region (stress is almost constant with increase in strain) and densification region (stress increases rapidly with strain). Plateau stress

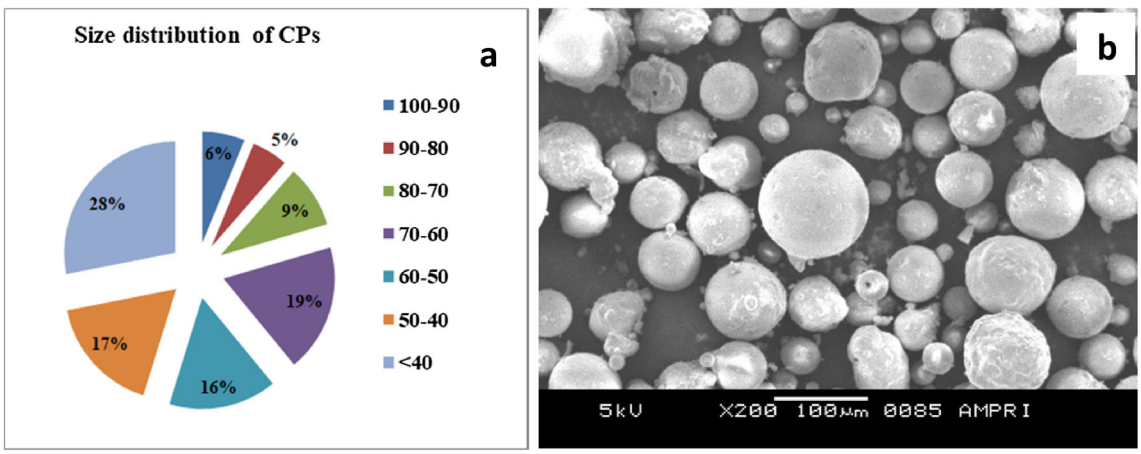

Fig. 1 **a** Size distribution of added CPs, **b** microstructure of CPs

Table 1 Properties of Zn–8Al hybrid foam at constant temperature and varying strain rates

Group	Temp (°C)	SR (s^{-1})	Weight (g)	Density (g/cc)	RD	σ_{pl} (MPa)	E_{ab} (MJ/m^3)	ε_d	σ_{Max} (MPa)	η
G-1	100	0.01	21.81	1.40	0.27	3.14	2.17	0.69	4.47	0.70
		0.1	21.92	1.40	0.27	3.65	2.52	0.69	4.61	0.79
		1	21.79	1.39	0.27	3.95	2.77	0.70	5.01	0.79
G-2	100	0.01	17.98	1.15	0.22	2.41	1.69	0.70	4.07	0.59
		0.1	17.79	1.14	0.22	2.52	1.71	0.68	4.32	0.58
		1	17.72	1.13	0.22	2.68	1.85	0.69	3.95	0.68
G-3	100	0.01	14.83	0.95	0.18	1.51	1.06	0.70	2.14	0.71
		0.1	14.84	0.95	0.18	1.57	1.08	0.69	2.51	0.63
		1	14.72	0.94	0.18	1.72	1.19	0.69	2.62	0.66

considered as the average stress during plateau region up to densification strain is reported in Tables 1 and 2.

The energy absorption capacity (EAC) was calculated by the following relation:

$$E_{ab} = \int_0^{\varepsilon_d} \sigma_{pl}(\varepsilon)\mathrm{d}\varepsilon \tag{1}$$

where E_{ab} is EAC, ε_d is densification strain (DS) and σ_{pl} is PS.

And the energy absorption efficiency (η) was calculated by the following relationship:

$$\eta = \frac{\int_0^{\varepsilon_d} \sigma(\varepsilon)\mathrm{d}\varepsilon}{\sigma_{max} \times \varepsilon_d} \tag{2}$$

3 Results

3.1 Relative Density and Scanning Electron Microscopy

Cube samples of 25-mm dimension were sliced from the foam ingot, and RD of hybrid foam was measured by the ratio of the density of foam to the density of the composite. The density was found in the range of 0.94–1.40 g/cm^3, and the density of the composite was calculated using the rule of the mixture and found to be 5.16 g/cm^3. The RD of the hybrid foam was found to be 0.27, 0.22 and 0.18. Each set of RD was examined under varying SR and temperature to find out compression deformation behavior of Zn–8Al hybrid foam. It was noted that higher RD gave higher compressive strength. The microstructural characterization of hybrid foam was carried out with the scanning electron microscope (SEM) model Hitachi-3600 installed at National Institute of Technology, Srinagar, India. The digital images of the microstructure are shown in Fig. 2; the CPs were reported by arrows in red color. The cell and cell wall of the hybrid foam were indicated by 'C' and 'CW' respectively. Figure 2a represents the single cell of the hybrid foam containing CPs accumulated into the structure. Figure 2b represents the dispersion of CPs at the cell wall, and Fig. 2c represents the *size of CPs* dispersed at the cell walls found in the range of 42.90–63.47 μm as the majority of CPs were in the range of < 40–70 μm as shown in Fig. 1a. The microstructure of the hybrid foam shows the distribution of CPs into the cell wall.

Table 2 Properties of Zn–8Al hybrid foam at constant strain rate and varying temperatures

Group	Temp (°C)	SR (s^{-1})	Weight (g)	Density (g/cc)	RD	σ_{pl} (MPa)	E_{ab} (MJ/m^3)	ε_d	σ_{Max} (MPa)	η
G-4	150	0.01	21.78	1.39	0.27	3.02	2.11	0.70	4.29	0.70
			17.94	1.15	0.22	2.35	1.65	0.70	4.05	0.58
			14.81	0.95	0.18	1.43	1.04	0.73	2.19	0.65
G-5	200	0.01	21.82	1.40	0.27	2.76	1.96	0.71	4.03	0.68
			17.85	1.14	0.22	2.10	1.45	0.69	3.05	0.69
			14.83	0.95	0.18	1.29	0.92	0.71	1.79	0.72
G-6	250	0.01	21.79	1.39	0.27	2.69	1.88	0.70	2.98	0.90
			17.91	1.15	0.22	1.87	1.33	0.71	3.20	0.58
			14.81	0.95	0.18	1.20	0.88	0.73	2.15	0.56

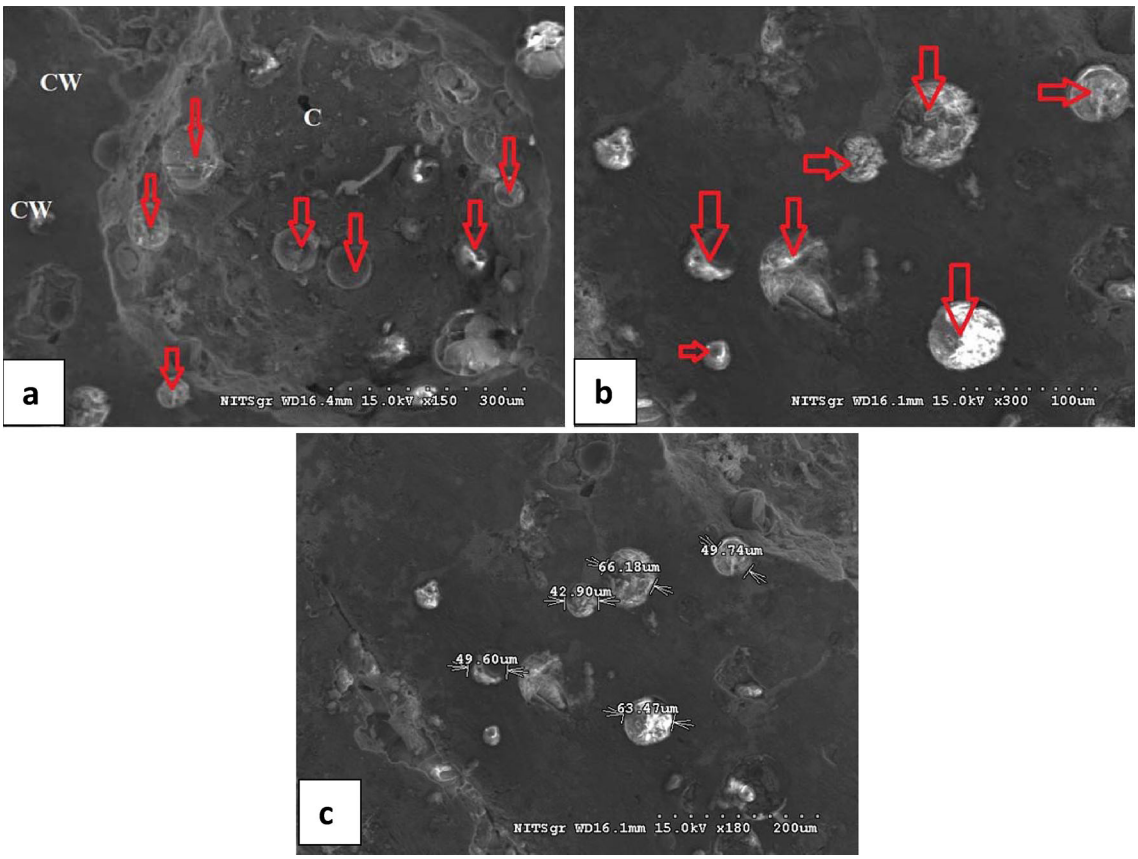

Fig. 2 Microstructure of hybrid foam

3.2 Compressive Deformation

3.2.1 Effect of Relative Density

The properties of the Zn–8Al hybrid foam evaluated from the compression test are reported in Tables 1 and 2. The effect of RD was examined at constant temperature and SR. Figure 3 represents the relation between RD and PS. It was noted that PS and EAC increased with RD. The PS was found to be 1.51, 2.41 and 3.14 for 0.18, 0.22 and 0.27 RD, respectively, for the compression test carried out at 100 °C and at 0.01 s^{-1} SR. The same phenomenon was noted for 0.1 and 1 s^{-1} SR. The densification had no effect with RD.

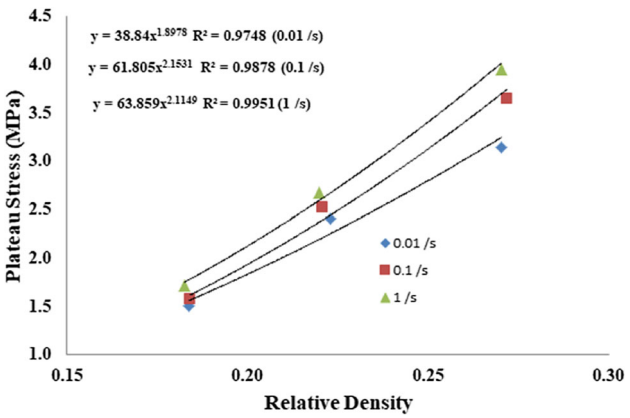

Fig. 3 Relation of plateau stress with relative density

3.2.2 Effect of Strain Rate

The samples of different relative densities were examined under constant temperature (100 °C) with varying strain rates (0.01, 0.1 and 1 s^{-1}). The values of PS, EAC and DS are reported in Table 1. The effect of SR on PS, EAC and DS is represented in Fig. 4a–c. It was observed that PS and EAC increased with increase in SR. The PS increased by 25.79, 11.20 and 13.90% for 0.27, 0.22 and 0.18 RD, respectively, and EAC increased by 27.64, 9.46 and 12.26% for the same RD. The DS was found to remain almost unchanged with increasing SR.

3.2.3 Effect of Temperature

To find out the effect of temperature on the deformation behavior of Zn–8Al hybrid foam, the experiments were carried out at constant SR (0.01 s^{-1}) by varying temperatures from 100 to 250 °C. It was noted that compressive

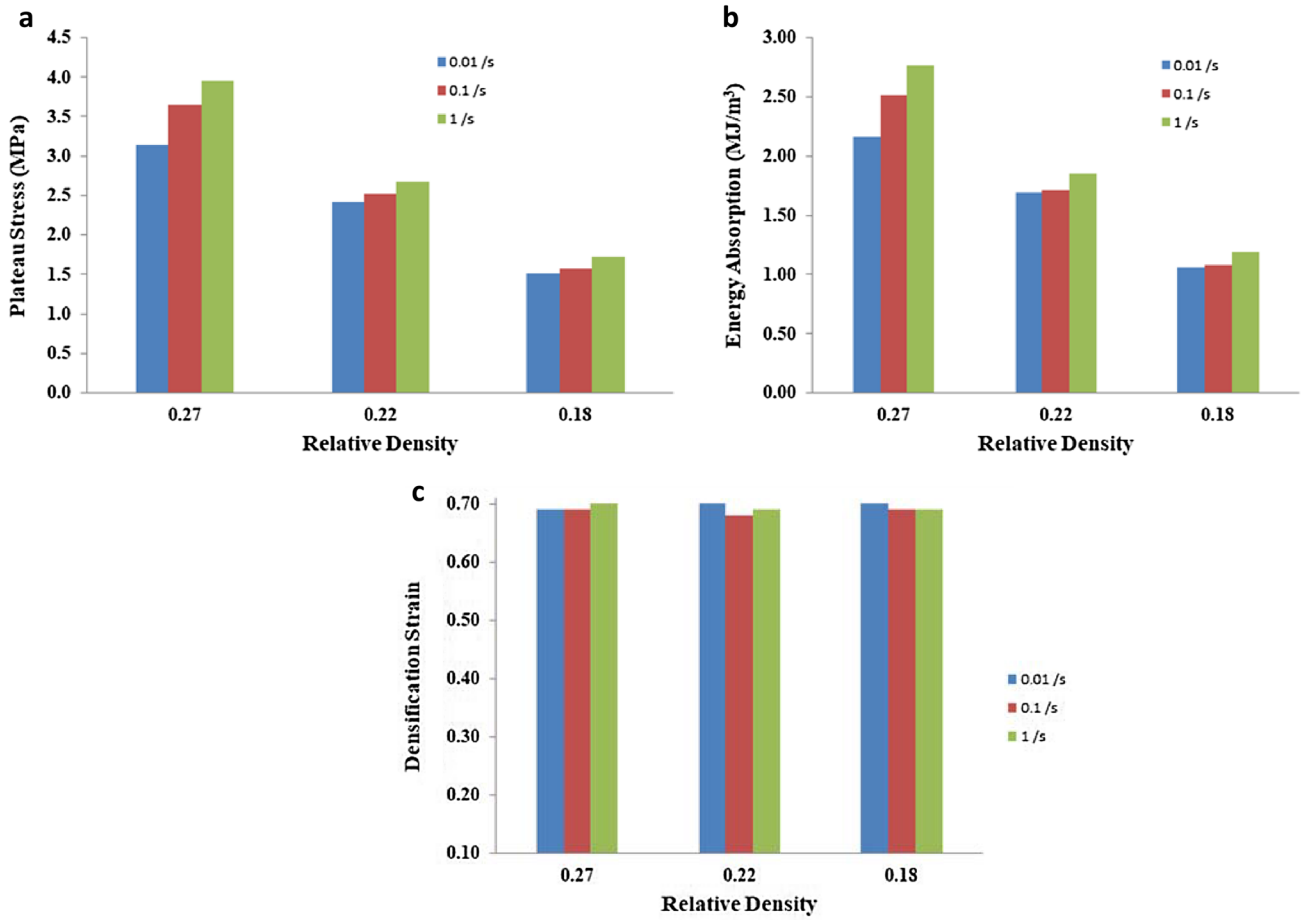

Fig. 4 Relation of relative density with strain rate for **a** plateau stress, **b** energy absorption and **c** densification strain

strength and EAC reduced with an increase in temperature for 0.27, 0.22 and 0.18 RD. The percentages of reduction in PS were observed to be 14.33, 22.40 and 20.52% for the existing set of RD and EAC got reduced by 13.36, 21.30 and 16.98%. The value of DS varied from 0.70 to 0.71; however, it was noted to be 0.73 for 0.18 RD at 150–250 °C. The bar chart for the PS, EA and DS is represented in Fig. 5a–c.

3.2.4 Energy Absorption Efficiency

The energy absorption efficiency (EAE) of the Zn–8Al hybrid foam was calculated by the relation described as in Eq. 2. It was found that the EAE of the hybrid foam was not stable for RD, temperature and SR. The efficiency was found to be in the range of 58–79% for the compression test performed at constant temperature (100 °C) by varying SR from 0.01 to 1 s^{-1} and 56 to 90% for the hybrid foam examined at constant SR (0.01 s^{-1}) by varying temperatures as 150–250 °C. The stress–strain curve for the EAE 90% and 56% is shown in Fig. 6.

4 Discussion

4.1 Relative Density

The RD of the synthesized hybrid foam through stir-casting varied from 0.18 to 0.27 due to the variation of temperature during foaming operation. The synthesis of the Zn–8Al hybrid foam with CPs as a thickening agent and CaH_2 as a foaming agent was performed in a cast iron crucible. For the uniform mixing of the foaming agent into the melt, mechanical stirrer was used for 3–4 min. The foaming temperature was maintained from 580 to 600 °C followed by solidification of molten foam. Higher foaming temperature resulted in lower RD due to the high expansion of hydrogen gas released through the decomposition of foaming agent.

4.2 Microstructural Evaluation

The dispersion of the CPs on the cell wall of the synthesized foam was present in the structure because of continuous stirring during mixing into the melt, and it showed

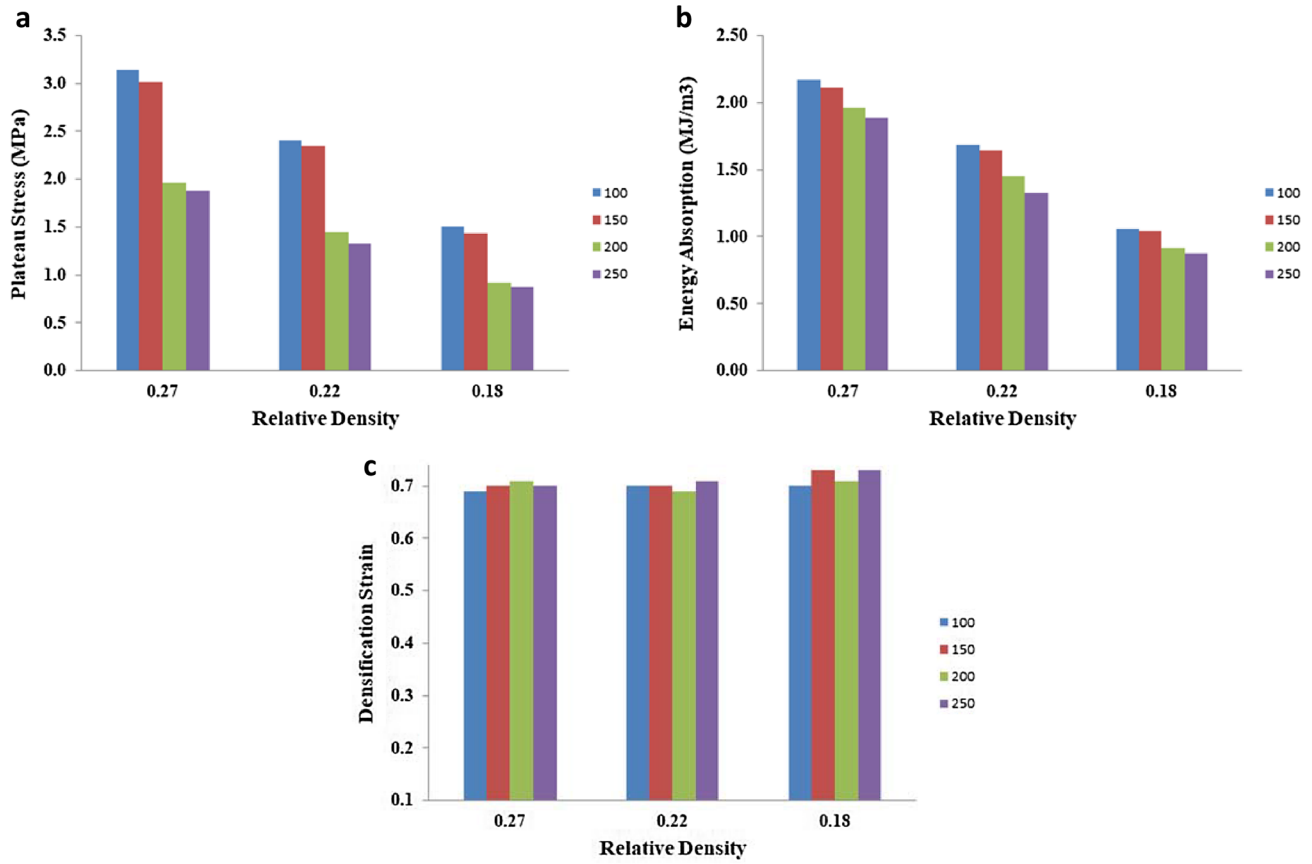

Fig. 5 Relation of relative density with temperature for **a** plateau stress, **b** energy absorption and **c** densification strain

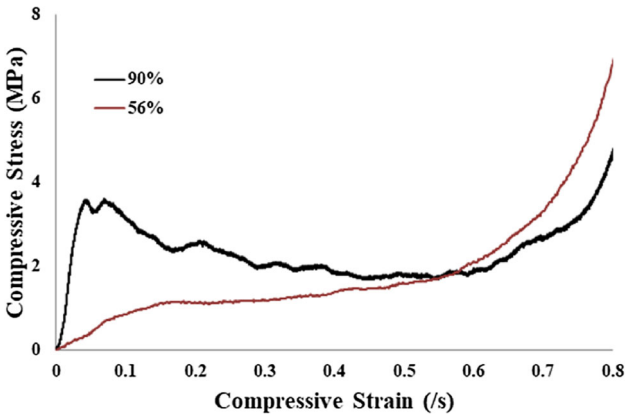

Fig. 6 Energy absorption efficiency

the hybrid behavior due to dual porosity present in the structure: the macroporosity due to entrapment of gas bubbles into liquid metal during solidification and the microporosity present due to the dispersion of CPs (hollow microballoons) at cell wall. The presence of CPs made the foam more light in weight and reduced the requirement of the costly foaming agent due to space holding characteristics. Reinforcement of CPs also increased the compressive strength and EAC of the hybrid foam.

4.3 Compressive Deformation Behavior

4.3.1 Effect of Relative Density

The compression tests were performed on three different relative densities, and results showed that higher RD gave higher compressive strength in terms of PS. The PS was observed as 3.14 MPa for 0.27 RD, while deformation of hybrid foam took place at 100 °C with 0.01 s^{-1} SR, and it got reduced to 1.51 MPa for the 0.18 RD for the same condition. The foam with 0.27 RD was less porous in comparison with 0.18 RD. Higher porosity resulted in less compressive strength due to less content of matrix material, but it was lighter in weight. The other reason for higher compressive strength for high RD was more cell wall thickness and lower cell size.

4.3.2 Effect of Strain Rate

It was noted that PS and EAC of the synthesized hybrid foam increased almost linearly with SR. The SRS was measured with the linear slope between ln (plateau stress) and ln (strain rate) as shown in Fig. 7a–c. The Zn12Al composite foam was examined at various SR, CPs with two

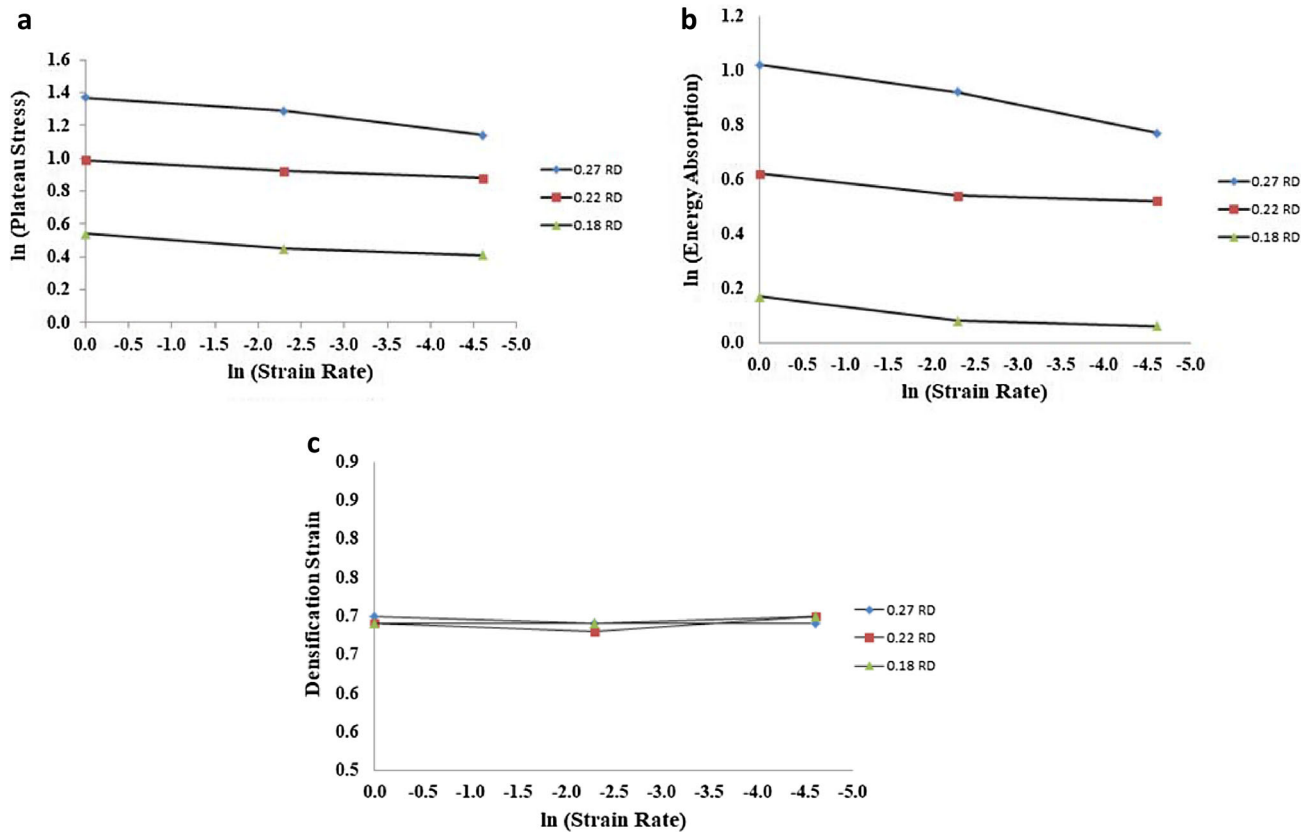

Fig. 7 Strain rate effect on **a** plateau stress, **b** energy absorption and **c** densification strain

different volume percents (15 and 30) and reported high SR sensitivity 0.42 and 0.5 for 15 and 30 vol% CPs, respectively [16]. The SRS of the ZnAl27 hybrid foam was measured and found in the range of 0.036–0.017 using CPs (20 vol%) [17]. In the present study, we found that SRS was in the range of 0.024–0.05, and the slope was found out with the best linear plots of ln (plateau Stress) v/s ln (strain rate). The synthesized foam was noted to be sensitive to the SR because of higher ductility of the matrix from which it was made of. The elastic behavior of the Zn–8Al hybrid foam made it suitable for use in energy absorption and high strain rate applications.

4.3.3 Effect of Temperature

The effect of temperature on PS, EAC and DS is reported in Fig. 8a–c, and it was noted that PS and EAC decreased with increase in temperature during compression test, but in hybrid foam, PS existed as 2.69, 1.87 and 1.20 MPa at 250 °C for the 0.27, 0.22 and 0.18 RD, respectively. PS of ZnAl27 hybrid foam having RD 0.27 was obtained as 2.21 MPa [17] and it was 2.84 MPa for ZnAl12 hybrid foam [18] at 250 °C for 0.01 s^{-1} with same volume fraction (20%) of CPs under compressive loading. The PS obtained in the present study was more than ZnAl27 hybrid foam and less than the ZnAl12 hybrid foam; this might be due to the variation of cell size and cell wall thickness. The PS and EAC were reported for ZnAl27 alloy with 10 wt% of SiC [12] and were better as compared to CPs due to good wettability of SiC particles and higher density. The compressive deformation behavior of ZnAl alloys with CPs might be improved by changing the process parameter. The DS remained almost invariant to the temperature as it varied in the range of 0.70–0.73 as reported in Table 2 due to variation in the level of porosity; however, it increased at a higher temperature because of matrix softening. A higher temperature during compression test resulted in lower compressive strength due to extra heat energy applied to the specimen, and it lost its strength.

4.3.4 Energy Absorption Efficiency

Tables 1 and 2 reported EAE of Zn–8Al hybrid foam for 0.27, 0.24 and 0.18 RD. The EAE of the hybrid foam was found in the random range of 56–90%. The EAE for ZnAl27–SiC foam was reported in the range of 98.6–60.8 [12]. The reported values of EAE for ZnAl27 and ZnAl12 hybrid foam [17, 18] were in the range of 70–96% and 51–94%, respectively. EAE obtained from the present study was comparatively less from the reported literature due to

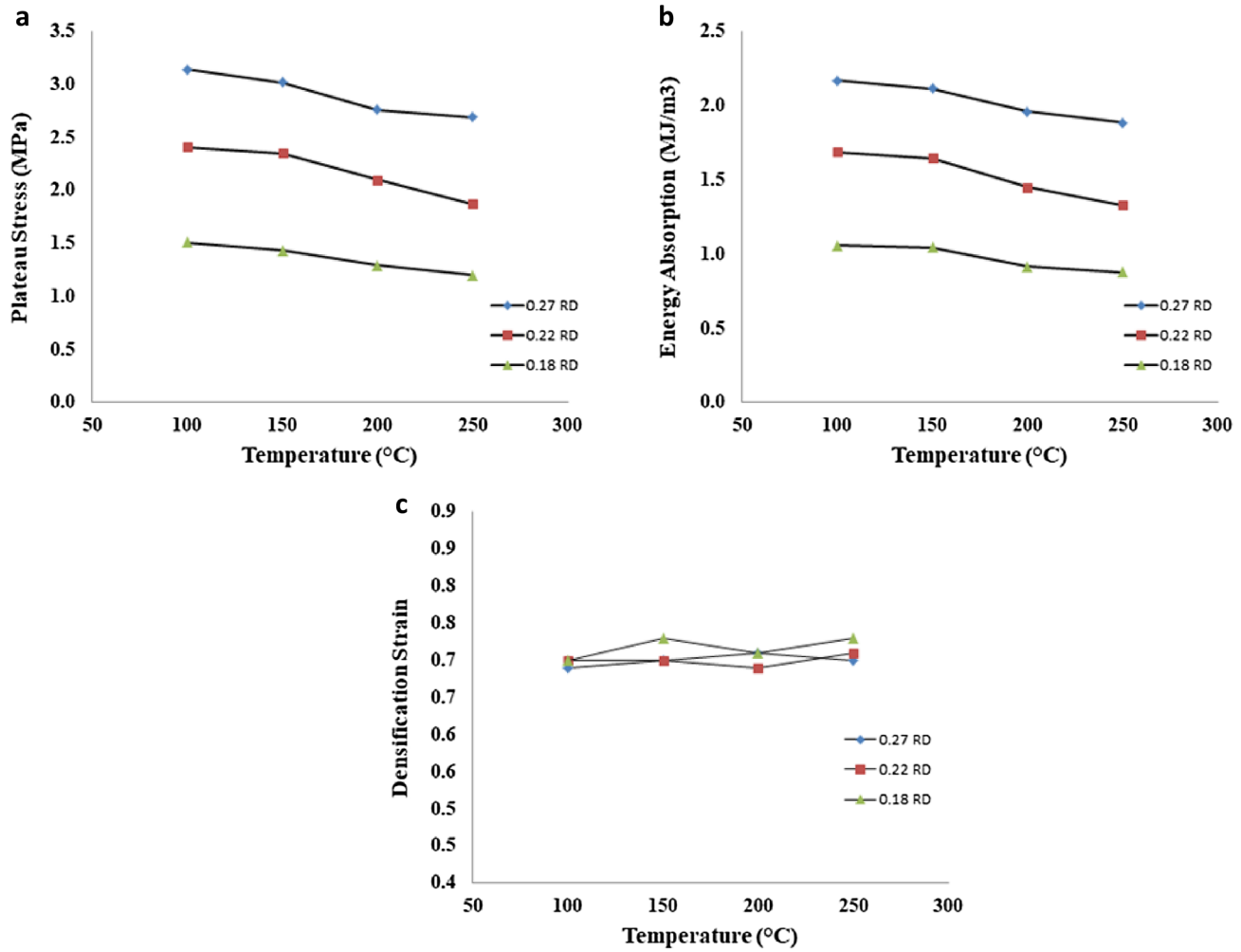

Fig. 8 Temperature effect on **a** plateau stress, **b** energy absorption and **c** densification strain

the presence of some coarser cells in the foam structure. A higher difference between PS and maximum stress resulted in a reduction in EAE. Moreover, it also depended on the product of the maximum stress and DS; increase in the product of σ_{max} and ε_d resulted in lower EAE. It could be improved with the uniform cell size and distribution of the cells into the structure which resulted in more flat plateau region to reduce the difference between σ_{max} and PS.

5 Conclusions

1. Zn–8Al hybrid foam was synthesized successfully using CPs as a thickening agent and CaH_2 as the foaming agent through stir-casting technique.
2. The densities of hybrid foam were found in the range of 0.94–1.40 g/cm^3 which was much less than the density of the matrix (Zn–8Al) 6.3 g/cm^3 and that of composite 5.16 g/cm^3. The level of porosity was found to be 88–73%.
3. The microstructural characterization showed that CPs were distributed at the cell walls of the hybrid foam.
4. The strain rate sensitivity of the hybrid foam was calculated from (0.024–0.05) and made it suitable for applications at higher strain rate.
5. The plateau stress and energy absorption capacity of samples were increased with relative density and strain rate, whereas reduced phenomenon was observed with an increase in temperature during compressive deformation.
6. The energy absorption efficiency of samples was found in the range of 56–90%.

References

1. Degischer H P, Kriszt B, *Handbook of Cellular Metals—Production, Processing, Applications* (2002). https://doi.org/10.1002/3527600558.fmatter_indsub.

2. Balch D K, Dunand D C, *Acta Mater* **54** (2006) 1501. https://doi.org/10.1016/j.actamat.2005.11.017.
3. Wu G H, Dou Z Y, Sun D L, Jiang L T, Ding B S, He B F, *Scr Mater* **56** (2007) 221. https://doi.org/10.1016/j.scriptamat.2006.10.008.
4. Licitra L, Luong D D, Strbik O M, Gupta N, *Mater Des* **66** (2015) 504. https://doi.org/10.1016/j.matdes.2014.03.041.
5. Mondal D P, Jha N, Badkul A, Das S, Khedle R, *Mater Sci Eng A* **534** (2012) 521. https://doi.org/10.1016/j.msea.2011.12.002.
6. Tao X F, Zhao Y Y, *Scr Mater* **61** (2009) 461. https://doi.org/10.1016/j.scriptamat.2009.04.045.
7. Mamatha T G, Patnaik A, Biswas S, Satapathy B K, Redhewall A K, *Comput Mater Sci* **55** (2012) 100. https://doi.org/10.1016/j.commatsci.2011.11.028.
8. Shivakumar N, Vasu V, Narasaiah N, Kumar S, *Procedia Mater Sci* **10** (2015) 159. https://doi.org/10.1016/j.mspro.2015.06.037.
9. Fatile B O, Adewuyi BO, Owoyemi H T, *Eng Sci Technol Int J* 20 (2017) 1147. https://doi.org/10.1016/j.jestch.2017.01.001.
10. Yu S, Liu J, Luo Y, Liu Y, *Mater Sci Eng A* **457** (2007) 325. https://doi.org/10.1016/j.msea.2006.12.089.
11. Mondal D P, Goel M D, Bagde N, Jha N, Sahu S, Barnwal A K, *Mater Des* **57** (2014) 315. https://doi.org/10.1016/j.matdes.2013.12.026.
12. Sahu S, Goel M D, Mondal D P, Das S, *Mater Sci Eng A* **607** (2014) 162. https://doi.org/10.1016/j.msea.2014.04.004.
13. Kitazono K, Sekido K, *Procedia Mater Sci* **4** (2014) 175. https://doi.org/10.1016/j.mspro.2014.07.586.
14. Gui M C, Wang D B, Wu J J, Yuan G J, Li C G, *Mater Sci Eng A* **286** (2000) 282. https://doi.org/10.1016/s0921-5093(00)00789-9.
15. González Nava M, Cruz-Ramírez A, Ángel Suarez Rosales M, Gutiérrez-Pérez V H, Sánchez-Martínez A, *J Alloys Compd* **698** (2017) 1009. https://doi.org/10.1016/j.jallcom.2016.12.170.
16. Daoud A, *Mater Sci Eng A* **525** (2009) 7. https://doi.org/10.1016/j.msea.2009.05.038.
17. Manoj, Afzal Khan D M, Mondal D P, *Mater Sci Eng A* **731** (2018) 324. https://doi.org/10.1016/j.msea.2018.06.044.
18. Manoj, Afzal Khan D M, Mondal D P, *Mater Res Express* **5** (2018) 116507. https://doi.org/10.1088/2053-1591/aadcc9.
19. Birla S, Mondal D P, Das S, Kashyap D K, Ch V A N, *Mater Sci Eng A* **685** (2017) 213. https://doi.org/10.1016/j.msea.2016.12.131.
20. Birla S, Mondal D P, Das S, Khare A, Singh J P, *Mater Des* **117** (2017) 168. https://doi.org/10.1016/j.matdes.2016.12.078.